Nanoscale

RSC Publishing

REVIEW

View Article Online
View Journal | View Issue

Cite this: *Nanoscale*, 2013, **5**, 5677

Plasmonic nanocomposites: polymer-guided strategies for assembling metal nanoparticles

Bo Gao, Matthew J. Rozin and Andrea R. Tao*

Noble metal nanoparticles that support localized surface plasmon resonances (LSPRs) have the unique ability to manipulate and confine light at subwavelength dimensions. Utilizing these capabilities in devices and coatings requires the controlled organization of metal nanoparticles into ordered or hierarchical structures. Polymer grafts can be used as assembly-regulating molecules that bind to the nanoparticle surface and guide nanoparticle organization in solution, at interfaces, and within condensed phases. Here, we present an overview of polymer-directed assembly of plasmonic nanoparticles. We discuss how polymer grafts can be used to control short-range nanoparticle interactions that dictate interparticle gap distance and orientation. We also discuss how condensed polymer grafts can be used to control long-range order within condensed nanoparticle–polymer blends. The assembly of shaped plasmonic nanoparticles that have potential applications in enhanced spectroscopy and optical metamaterials is highlighted. We end with a summary of promising new directions toward the fabrication of plasmonic nanocomposites that are responsive and possess three-dimensional order.

Received 4th March 2013
Accepted 3rd May 2013

DOI: 10.1039/c3nr01091k

www.rsc.org/nanoscale

1 Introduction

Metal nanoparticles composed of Au and Ag behave like optical antennae by supporting the excitation of localized surface plasmon resonances (LSPRs), where conduction electrons of the metal oscillate in resonance with the incident light wave to produce intense electromagnetic fields localized at the metal surface. The size, shape, and arrangement of plasmonic metal nanoparticles are critical in determining the LSPR wavelength and the magnitude of the resulting field enhancement. *Hot spots*—where the electromagnetic field is highly confined within a small volume—are particularly pronounced at sharp nanoscale features (*i.e.* the antenna effect) and small gaps between adjacent metal surfaces. To utilize this plasmonic field enhancement within a device, hot spots must be fabricated with controlled densities and locations. Thus, arrays of nanoparticles are typically desired. For example, periodic arrays of metal nanoparticles deposited at an absorber interface can serve as plasmonic concentrators in a photovoltaic device[1] and two-dimensional (2D) arrays of nanoscale split-ring resonators[2]

NanoEngineering Department, University of California, San Diego, 9500 Gilman Dr #0448, La Jolla, CA 92093-0448, USA. E-mail: atao@ucsd.edu; Fax: +1-858-5349553; Tel: +1-858-8224237

Bo Gao received her B.S. in Chemistry in 2002 from Fudan University in China. She obtained her Ph.D. in Chemistry from University of Notre Dame in 2009 exploring nanoscale patterning of biomolecules by e-beam lithography. She is currently a postdoctoral scholar in the Tao Group in the Nano-Engineering Department at the University of California, San Diego. Her research interests include self-assembly, nanoparticle–polymer composite, plasmonics, nanofabrication and biosensing.

Matthew Rozin received his B.S. in Chemical Engineering from the University of Massachusetts Amherst in 2010. He is currently a second year Ph.D. student with the Tao Group in the Nano-Engineering Department at the University of California, San Diego. He is working on large-scale polymer directed nanoparticle assembly for plasmonic metamaterials.

and paired metal stripes[3] have been demonstrated as negative-index metamaterials.

Self-assembly provides a bottom-up approach to the fabrication of plasmonic arrays and has the potential to accommodate massively parallel, large-scale materials processing for device integration. Specifically, nanoparticle organization can be engineered for specific optical functions, for example: chains for waveguiding;[4] tapers and gaps for focusing;[5] grooves and apertures for transmission;[6] and clusters for negative refractive index metamaterials.[7] In addition, ensembles of nanoparticles can support SP excitation over multiple length scales—from a few nanometers for LSPRs to tens of microns for long-range propagating surface plasmons—and may enable the observation of unique emergent optical properties. A significant challenge in the self-assembly of metal nanoparticles is the formation of non-close-packed nanoparticle groupings that possess hierarchical order and specific interparticle orientations. Towards this end, a variety of self-assembly strategies for colloidal metal nanoparticles have been explored for the fabrication of plasmonic materials, including capillary or convective assembly, assembly at fluid interfaces, and chemical tethering between nanoparticles.[7a,8]

Polymer-directed assembly is a particularly attractive route for the organization of colloidal metal nanoparticles into plasmonic groups and arrays. In these strategies, Ag and Au nanoparticles whose surfaces are grafted with polymer chains can be organized into clusters, chains, micelles, and other complex structures. Assembly is guided by intermolecular forces rather than strong chemical bonds between nanoparticles. Generally, these nanoparticle assemblies form by approaching equilibrium, where variables such as polymer graft length, graft density, and miscibility are important parameters in determining the energy of interaction between nanoparticles. In this manner, polymer grafts can be selected to control the spacing between nanoparticles, the orientation of shaped nanoparticles, or the long-range order of nanoparticles dispersed within a polymer matrix. The formation of nanocomposite materials is particularly attractive not only because the polymer matrix provides a convenient dielectric medium for encapsulation of the plasmonic nanoparticles, but also because it enables the use of polymeric processing techniques (*e.g.* extrusion, molding, thin-film casting) that are amenable for large-scale manufacturing of these electromagnetic materials.

In this review article, we will summarize research in the polymer-directed assembly of plasmonic nanoparticles. We will focus our discussion to the assembly of metal nanoparticles composed of Ag and Au, although we recognize that semiconductor quantum dots and graphene also have great potential as plasmonic building blocks.

2 Grafting the nanoparticle surface

Plasmonic nanoparticles are typically surface-modified with polymer grafts during nanoparticle synthesis or in a post-synthetic ligand exchange step. For modification *in situ*, surface functionalization is carried out during the nanoparticle synthesis by introducing the desired polymer graft into the reaction mixture (Fig. 1a). The polymer can serve a double role as both a shape-directing molecule and a surface passivating agent during the synthesis. For example, the polyol process is a common approach to synthesizing colloidal Ag and Au nanoparticles by carrying out metal reduction in a diol solvent. Poly(vinyl pyrrolidone) (PVP) is generally added during the reduction of a metal salt. PVP is known to behave as a stabilizing agent for the lowest energy crystal faces of Ag and Au (*e.g.* the {111}, {100}, and {110} planes), and promotes the formation of polyhedral nanoparticles.[9] The resulting polyhedral nanoparticles are well-protected by PVP chains, which are grafted to the metal surface through interaction with their pyrrolidone functional groups. While polymer grafting density is poorly controlled in this reaction, it is likely that the polymer chains adopt a brush-like structure at the metal surface given the typical lengths of the PVP chains (M_w = 29k to 200k) employed in these synthesis.[9,10]

Similarly, Ag and Au nanoparticles can be synthesized in the presence of cationic polyelectrolytes to produce crystalline nanoparticles with a narrow size-distribution.[11]

Andrea Tao is an Assistant Professor in the NanoEngineering Department at the University of California, San Diego. She earned her A.B. in Chemistry and Physics from Harvard University in 2002, and her doctoral degree in Chemistry from UC Berkeley in 2007 exploring the self-assembly of inorganic nanoparticles. Prior to joining UCSD in 2009, Andrea spent two years as a UC President's Post-Doctoral Fellow at UC Santa Barbara uncovering new biological self-assembling systems in the optical proteins of octopus and squid. Currently, her research group focuses on the discovery and development of rational chemical frameworks for engineering solid-state nanomaterials.

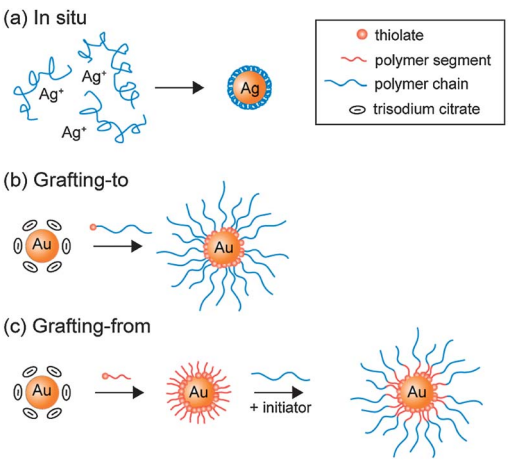

Fig. 1 Schematic illustration of polymer grafting strategy on nanoparticle surfaces.

Polyelectrolyte-stabilized nanoparticles are prepared *via* the rapid addition of a fast reducing agent such as potassium borohydride (KBH_4) to an aqueous solution of a metal salt (such as $AgNO_3$ or $HAuCl_4$) and excess polyelectrolyte.[11] *In situ* modification is dependent on the polyelectrolyte's ability to form complexes with the metal cation, and various chloride-based cationic polyelectrolytes such as poly(diallyldimethylammonium chloride) and poly(2-hydroxy-3-methacryloxypropyltrimethyl ammonium chloride) are commonly used.[12] Polymer graft layers resulting from *in situ* nanoparticle modification with a polyelectrolyte tend to be limited to sub-monolayer shells surrounding the nanoparticles, since the polymers are inherently labile and must allow for nanoparticle nucleation and growth. Thicker polymer layers can be achieved by grafting metal nanoparticles with cross-linked amphiphilic copolymers, where shell thickness is controlled by tuning the nanoparticle to copolymer ratio in solution.[13] Nanoparticles can be modified post-synthesis through ligand exchange reactions that substitute the capping molecule of the as-made nanoparticle, or through chemical alteration of the capping molecule. For nanoparticles that serve as plasmonic building blocks, commonly used capping molecules include sodium citrate and various cationic surfactants such as cetyltrimethylammonium bromide (CTAB),[14] benzyldimethyl hexadecylammonium chloride,[15] or cetylpyridinium chloride monohydrate.[16] Because these capping molecules tend to be labile and only weakly chemisorbed to the nanoparticle surface, ligand exchange reactions are a versatile strategy for nanoparticle surface modification with polymer grafts (Fig. 1b). Displacement of the capping molecule is typically carried out by either: (i) covalent binding of the graft to the nanoparticle surface, or (ii) through physisorption of the polymer graft. The effectiveness of this displacement depends on the affinity of the polymer graft with the nanoparticle surface. Post-synthetic modification of the nanoparticle is typically limited to polymer grafts that display strong binding affinities to metal surfaces. For example, thiol-functionalized polymer grafts are widely used in the surface modification of plasmonic nanoparticles, since the high affinity of the thiol for Ag and Au enables facile end-tethering of the polymer to the metal nanoparticle surface.[17]

In order to modify the composition of the chemical grafts on the nanoparticle surface *in situ*, a grafting-from approach can be considered where polymers are grown from the nanoparticle surface *via* polymerization reactions (Fig. 1c). This technique is useful for building brush like or cross-linked ligand shells, with thickness on the order of or larger than the nanoparticle diameter. Responsive polymers can be utilized in a grafting-from approach to create smart core–shell particles or microgels that respond to external stimuli by shrinking or swelling. For example, growth of the poly-*N*-isopropylacrylamide (pNIPAM) shell around the Au nanoparticles has been demonstrated through precipitation polymerization on the Au nanoparticle surface using the monomer NIPAM and cross-linker.[18] Other polymers such as polystyrene (PS),[19] poly(vinyl alcohol) (PVA),[20] polystyrene-*block*-poly(acrylic acid) (PS-*b*-PAA),[21] polypyrrole,[22] and phenol formaldehyde resin[23] have also been successfully attached using a grafting-from approach.

3 Plasmonic nanojunctions

The enhanced electromagnetic field generated by surface plasmon is highly localized at the nanoparticle and decays exponentially away from the nanoparticle surface as a consequence of the highly bound, non-radiative nature of surface plasmon at the metal–dielectric interface. To produce a nanojunction that effectively confines light to a small volume, strong electromagnetic coupling must be generated between closely spaced nanoparticles with interparticle gaps of only a few nanometers. Interparticle separation distance is observed to have a profound effect on the resonant wavelength for which strong coupling is observed. While direct-write techniques such as electron-beam lithography can produce nanostructures with sub-10 nm separation distances,[24] achieving such spatial control with bottom-up assembly methods can present a difficult challenge.

Polymer grafts can be used as molecular spacers to control metal nanoparticle separation distances during the assembly process. By thoughtfully tailoring the length of the graft chain, inter-nanoparticle junctions can be tuned to control the degree of plasmonic coupling between nanoparticles (Fig. 2a). Moreover, compression of the grafts at short interparticle separation distances provides an entropic barrier to gap distances of zero (*i.e.* touching or fused nanoparticles). For example, spherical Au nanoparticles can be self-organized into 2D and 3D aggregates after surface modification with poly(oxypropylene)diamines (POPDAs). The amine groups on the difunctional polymer are bound to citrate coated Au nanoparticles through ligand exchange and act as a cross-linker to drive nanoparticle assembly. As molecular weight of the polymer is increased from

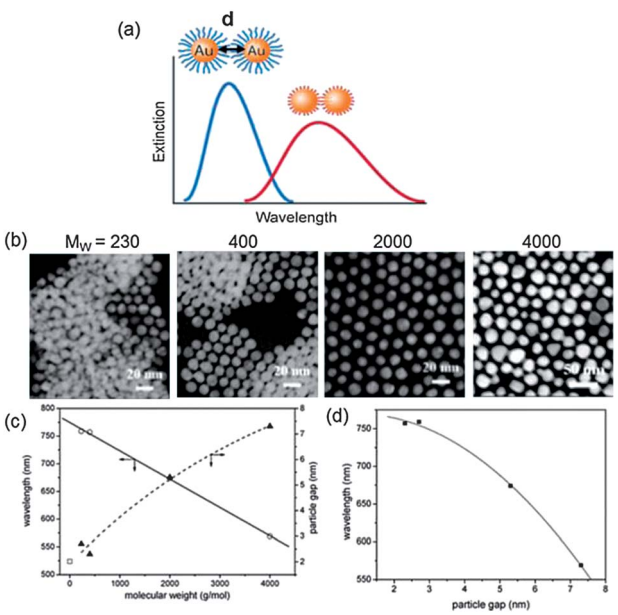

Fig. 2 (a) Schematic illustration of dependence of Au nanoparticle plasmonic coupling on grafted polymer chain length. (b) TEM images of Au nanoparticles modified with POPDA of different molecular weights. (c) Absorption band (circle) and particle gap (triangle) of Au nanoparticle change as a function of ligand molecular weight. (d) Gap dependence of the optical absorption of ligand-capped Au nanoparticles. Reproduced with permission from ref. 25.

230 to 4000 g mol^{-1}, the inter-nanoparticle distances in the nanoparticle aggregates are increased from 2.7 ± 0.7 nm to 7.3 ± 1.3 nm.[25] Correspondingly, the optical response of these aggregates shows a large blue-shift in LSPR wavelength from 759 nm to 569 nm (Fig. 2b–d).

In linear nanoparticle assemblies, this polymer-directed control over interparticle spacing has been demonstrated with nanometer precision. For example, spherical Au nanoparticles suspended in a mixture of ethanol and water can be aggregated to form chain-like assemblies by adding short thiol-terminated grafts with the formula $HS(CH_2)_nCOOH$, where n is number of methylene units in the graft. The interparticle spacings between adjacent Au nanoparticles are dependent on n, which was varied from 2–15 units to tune the interparticle spacing between 0.6 and 1.6 nm.[26] Smaller spacings give rise to a red-shift in the observed LSPR wavelength due to increased plasmon coupling, with a maximum shift of $\Delta\lambda = 97$ nm. Interparticle spacing can be further guided by utilizing a more rigid polymer backbone to facilitate nanoparticle assembly into chains (Fig. 3), which can increase the interparticle spacing up to 5.4 nm.[27]

Polymer grafts can also be utilized to fabricate dynamic, responsive plasmonic assemblies by employing grafts that exhibit adaptable chain lengths or conformations. For example, Au nanorods that are chemically modified by end-tethered photoactive polymers can be assembled into linear superstructures whose inter-rod spacings are controlled by solvent swelling.[28] The polymer grafts between neighboring nanorods are first photochemically cross-linked, resulting in a reduction of the inter-rod spacing of up to 55% and corresponding red-shift of $\Delta\lambda = 60$ nm in the LSPR wavelength. This red-shift occurs specifically for the longitudinal LSPR mode that is polarized along the nanorod main axis, since the nanorods are aligned end-to-end. Solvent-induced swelling of the cross-linked grafts can then be carried out to increase in the inter-rod distance, while maintaining the structural integrity of the chain-like nanorod assembly (Fig. 4b). Swelling of the cross-linked polymers weakens electromagnetic coupling between adjacent nanorods and leads to an observable blue-shift of the LSPR wavelength.

Using inter-nanoparticle spacing to induce dramatic changes in LSPR wavelength was further demonstrated by Qian *et al.* in the development of pH-responsive substrates for surface-enhanced Raman spectroscopy (SERS) (Fig. 4f). Au nanoparticles were grafted with a thiol-functionalized block copolymer (BCP) consisting of a pH-responsive polymethacrylic acid (PMAA) block ($M_w = 3000$) and an amphiphilic polyethylene glycol (PEG) block ($M_w = 5000$).[29] At pH < 4, the PMAA segment undergoes a reversible conformational change from an expanded chain to a collapsed structure, leading to a large decrease in interparticle distance and an increase electromagnetic coupling between nanoparticles. As a result of this hot spot generation, they observed large pH-dependent intensity changes for SERS reporter molecules located in the interparticle gaps.

For 3D plasmonic assemblies, controlled interparticle separation distances have been accomplished using the "brick-and-mortar" approach developed by the Rotello group, where a polymer dendrimer serves as the "mortar" or spacer layer

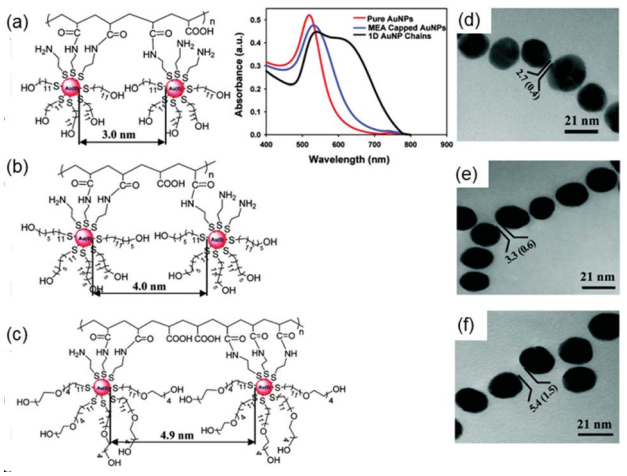

Fig. 3 (a–c) Schematic representations and corresponding TEM images (d–f) of the formation of 1D Au nanoparticle chains with different interparticle spacings based on using ligands with different lengths. (a) 11-Mercapto-1-undecanol, (b) 16-hydroxy-1-hexadecanethiol and (c) 1-mercaptoundecyl tetra(ethylene glycol). UV-vis absorption spectra of gold nanoparticles grafted with (a) at different stages of the chain formation process. Reproduced with permission from ref. 27.

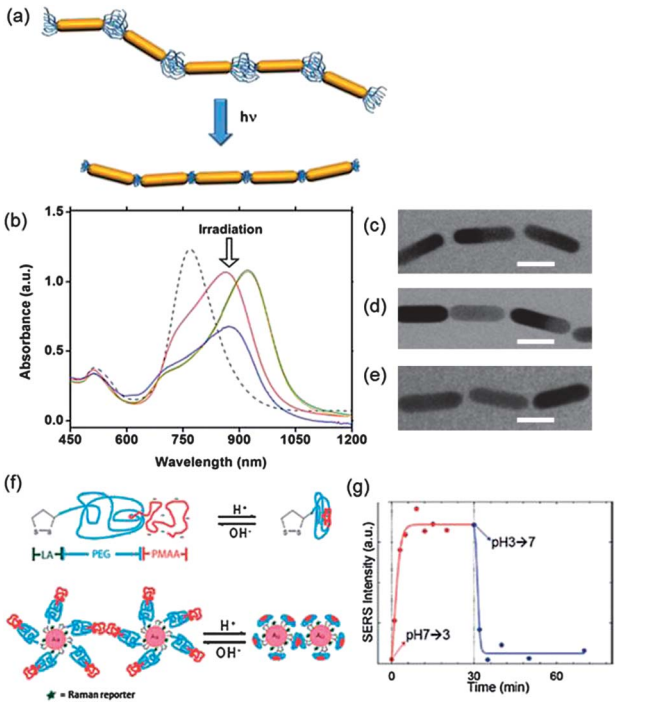

Fig. 4 (a) Schematic and (b) absorbance spectra of Au nanorods self-assemble into linear chains before and after photoirradiation with corresponding TEM images (c–e). Individual nanorods (dashed line), nanorod chains after self-assembly (red line, image c), 10 min (green line) and 19 h after photoirradiation (orange line, image d), and after dilution of the system with DMF (blue line, image e) Scale bars are 25 nm. Reproduced with permission from ref. 28. (f) Schematic structure of pH-induced conformational changes of a diblock copolymer PEG–PMAA with a terminal lipoic acid (LA) anchoring group. Au nanoparticles coated with LA–PEG–PMAA undergo reversible aggregation due to pH induced polymer conformational changes, leading to plasmonic coupling and (g) SERS signal intensity changes (at 1498 cm^{-1}) of reporter molecules. Reproduced with permission from ref. 29.

between neighboring Au nanoparticles.[30] Here, the polymer spacer can be physisorbed to the nanoparticle surface through electrostatic interactions. For example, an amine-terminated poly(amidoamine) (PAMAM) dendrimer can be physisorbed to the surface of Au nanoparticles covalently grafted with carboxylic acid terminated ligands (Fig. 5). The electrostatic interaction between the terminal amine on the dendrimer and the carboxylic acid on the nanoparticle surface provided the driving force for self-assembly. Increasing dendrimer diameter increases the interparticle separation distance between nanoparticles within the assembly. This is accompanied by a blue-shift in the optical extinction peak of the nanoparticle–dendrimer clusters due to weakened inter-nanoparticle electromagnetic coupling. The coupled LSPR mode is tunable over a range of $\Delta\lambda = 80$ nm for dendrimers between 0.6 and 1.9 nm in diameter.

Responsive polymers can also be utilized in a brick-and-mortar approach to fabricate 3D nanoparticle assemblies with dynamic optical properties. For example, bulk pNIPAM is well known for producing thermoresponsive gels that exhibit a reversible volume phase transition at its lower critical solution temperature (near 32 °C).[31] By heating and cooling an Au nanoparticle–pNIPAM nanocomposite near this temperature, shrinking and swelling of the spacer layer can give rise to reversible LSPR shifts[32] (Fig. 6). More recently, Au nanoparticles coated with a thick pNINAM shell (28 nm thick in the collapsed state at 45 °C and 37 nm thick in the swollen state at 25 °C) were assembled to produce 3D nanoparticle superlattices with tunable spacings over an impressive range, from 50 to 500 nm.[33] For the larger nanoparticle spacings, the ordered nanocomposites exhibit sharp peaks in their optical absorption spectra due to both LSPR excitation and optical diffraction effects. These nanoparticle–polymer core–shell assemblies display a fast melting and recrystallization response (<1 min) during heating and cooling cycles, and may provide a new pathway towards the fabrication of responsive, hybrid plasmonic–photonic crystals.

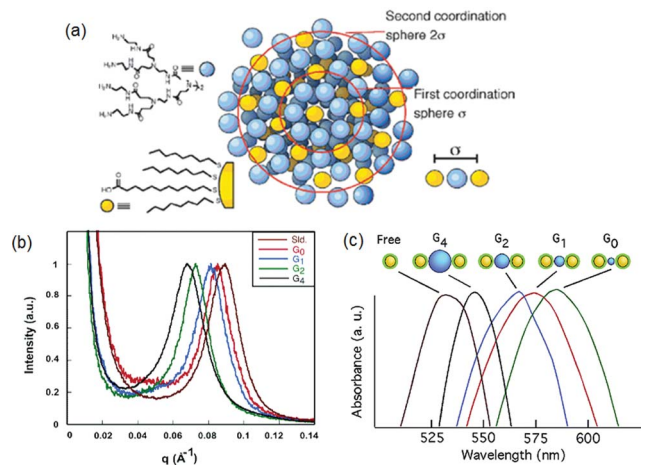

Fig. 5 (a) Schematic Au nanoparticles assembly using PAMAM dendrimers (blue sphere) as spacer; (b) small-angle X-ray scattering (SAXS) and (c) UV-visible studies on thin films of Au nanoparticles assembled with G0 through G4 dendrimers. Reproduced with permission from ref. 30.

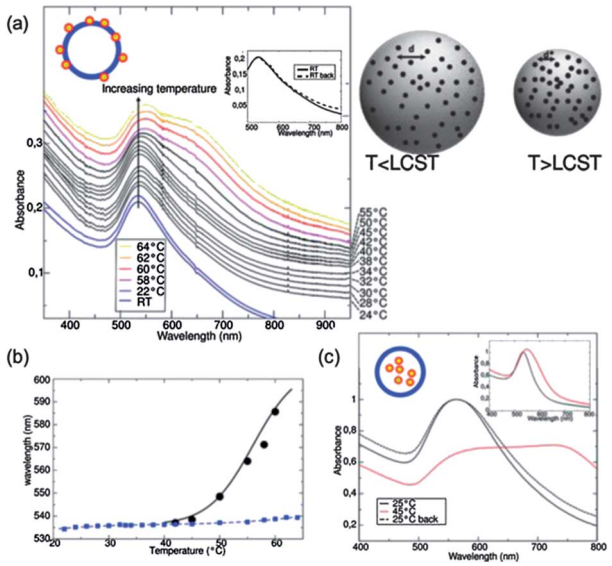

Fig. 6 (a) Absorption spectra of decorated Au–pNIPAM beads at different temperatures. Inset: comparison of spectra before heating and after cooling back to room temperature. The sketch showing swelling behavior of the beads (nanoparticles either on the surface or in the interior) at different temperature, the average distance *d* between the Au nanoparticles decreases upon pNIPAM sphere shrinkage. (b) Fundamental (squares) and coupled plasmon (circles) modes evolution with temperature for Au–pNIPAM spheres highly covered. (c) Absorption spectra of Au–pNIPAM beads with embedded Au particles of 40 nm diameter at 25 °C, 45 °C (red) and after cooling back to 25 °C. Inset: spectra for Au–pNIPAM spheres with 23 nm Au particles at 25 and 45 °C (red). Reproduced with permission from ref. 32.

4 Oriented plasmonic nanojunctions

A growing area of research in plasmonics is the assembly of shaped nanoparticle building blocks. Shaped metal nanoparticles possess LSPRs that can be tuned through chemical synthesis[34] and possess compelling geometries for constructing plasmonic nanojunctions by nanoparticle coordination through facet, corner, or edge sites.[35] Within these nanoparticle assemblies, electromagnetic coupling between neighboring nanoparticles is highly sensitive to nanoparticle orientation. For two approaching nanoparticles, van der Waals forces scale exponentially with the surface area of interaction.[36] As a result, shaped nanoparticles tend to organize into close-packed structures that maximize this interaction area: rods align side-by-side,[37] cubes align face-to-face (Fig. 7).[38] To control plasmonic coupling, nanoparticle assembly strategies must overcome these attractive van der Waals forces. As a result, significant efforts have been directed toward developing strategies for rationally assembling shaped nanoparticle building blocks into specific geometric orientations.

Here we discuss two general strategies for achieving specific nanoparticle orientations by employing a polymer graft to tune interparticle interactions: (i) site-selective modification, and (ii) homogeneous surface modification.

Site-selective modification

To overcome the tendency of nanoparticles to close-pack, the surface of a nanoparticle can be modified with polymer grafts

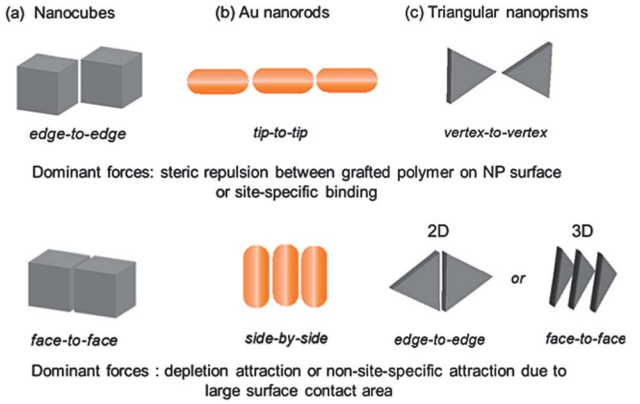

Fig. 7 Schematic illustration of oriented assembly of anisotropic plasmonic nanoparticles.

such that only certain site-specific interactions are allowed.[39] Site-selective modification can be achieved a number of different ways, including modification of nanoparticles with multiple polymer grafts that segregate into separate domains at the nanoparticle surface,[40] or by forming Janus-like particles through methods such as precipitate polymerization.[41] For plasmonic building blocks that possess different shapes, site-selective modification can take advantage of the inherent chemical anisotropy of the nanoparticle surfaces or facets that are present. This has been the most well-studied for Au nanorods, which are compelling plasmonic building blocks due to their shape-dependent LSPR excitations: Au nanorods are characterized by a longitudinal dipolar LSPR that oscillates along the major axis of the nanorod and a transverse dipolar LSPR that oscillates along the minor axis of the nanorod. Excitation of the longitudinal LSPR is responsible for the observed "lighting rod effect," where the electromagnetic field becomes focused at the nanorod tips upon irradiation with light. As a result, nanorod assembly in an end-to-end configuration is expected to result in a high degree of electromagnetic field confinement.

Several groups have succeeded in selectively tethering polymer chains to Au nanorod tips to form these desired architectures. Tip-selective modification involves a ligand exchange reaction that proceeds more readily at the nanorod tips, where the stabilizing surfactant layer is less dense and more readily displaced due to the high degree of curvature at ends of the nanorod relative to the nanorod side surfaces.[14] In the work of Nie *et al.*, nanorod tips are modified with thiol-terminated PS chains that render the tips hydrophobic. This pseudo-triblock structure (PS–surfactant–PS) can be triggered to assemble into different orientations by adjusting solvent conditions. Adding water—a bad solvent for PS—to a dispersion of the hybrid polymer–nanorod blocks in dimethyl formamide (DMF) produces end-to-end aligned nanorod chains, resulting in a redshift of λ_{LSPR} for the longitudinal SP mode.[42] On the other hand, the addition of water to a dispersion of nanorods in tetrahydrofuran (THF)—a bad solvent for the surfactant—produces nanorod bundles (Fig. 8). Further studies have explored the dynamic generation of plasmonic hot spots during the self-assembly process to establish a direct correlation

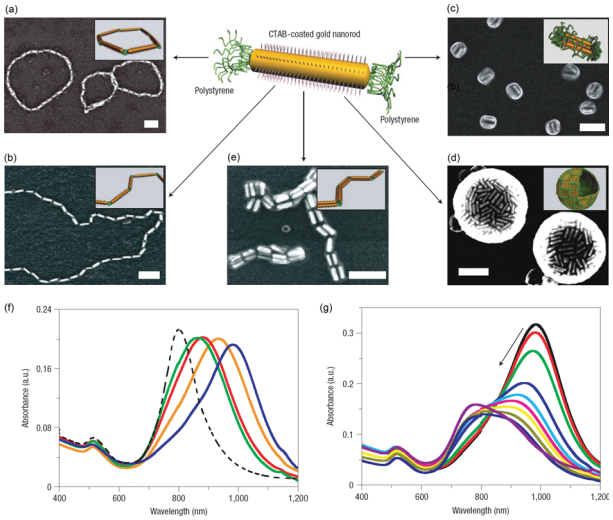

Fig. 8 Self-assembly of hydrophobic polymer end-tethered amphiphilic Au nanorods forming structures from rings to linear and bundled chains, and to nanospheres with 2D walls in selective solvents: (a and b) DMF–water mixture, (c and d) THF–water mixture, at water contents of 6 and 20 wt% respectively; and (e) ternary DMF–THF–water. The scale bars are 100 nm. UV-vis absorption spectra of (f) individual Au nanorods (dashed line) assemble into chains in DMF–water mixture with decreased water concentration (from left to right); (g) addition of THF into aqueous solution of nanorod chains as THF contents increases (from right to left). Reproduced with permission from ref. 42.

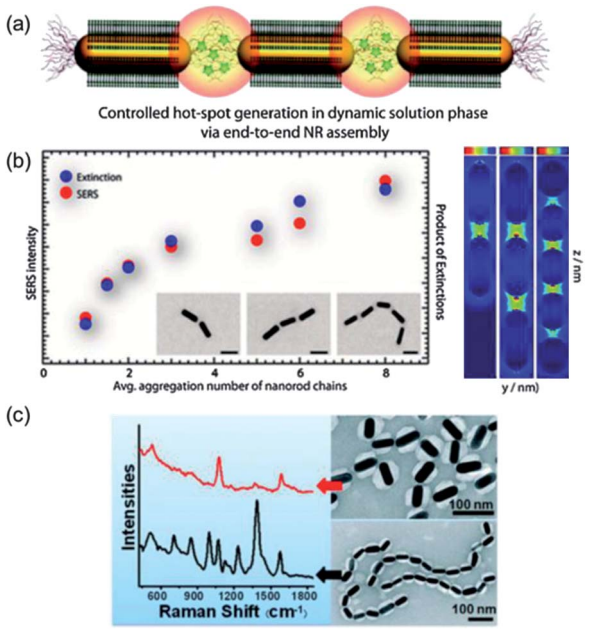

Fig. 9 (a) Schematics showing generation of hot-spots *via* end-to-end self-assembly of Au nanorods in chains in the presence of Raman reporter. The assembly is triggered by adding water to the solution of nanorods in DMF. (b) Correlation of the normalized intensity of SERS peak at 563 cm^{-1} (red circles) and the product of extinctions measured at 785 and 821 nm (blue circles) as a function of the average aggregation number of the nanorod chains. 3D finite-difference time-domain (3D-FDTD) simulation shows hot-spots formation between adjacent nanorods with maximum electric field intensity 4000 times greater than the incident field. Reproduced with permission from ref. 43. (c) SERS spectra change of 4-mercaptobenzoic acid adsorbed at the unprotected tips of PS-*b*-PAA coated nanorods before and after salt-induced linear aggregation of NRs (TEM images) due to molecular reorientation. Reproduced with permission from ref. 44.

between nanorod cluster sizes and ensemble-averaged SERS intensities[43] (Fig. 9). Chen *et al.* were able to generate SERS-active nanorod chains by selectively modifying the nanorod sides with PS-*b*-PAA grafts and leaving the nanorod tips bare.[44] They incorporated 4-mercaptobenzoic acid into the nanorod dispersions as a SERS analyte, and observed unusual changes in the SERS fingerprint generated by molecular reorientation in the hot spots (Fig. 9c).

Alternative routes for grafting polymers onto selective sites at the surface of a metal nanoparticle can involve a combination of top-down and bottom-up approaches. This can include surface modification of substrate-bound nanoparticles, where the substrate serves to protect a portion of the nanoparticle surface from exposure to a particular ligand or graft.[27,45] Another top-down method involves selective surface modification using a nano-contact printing approach. For example, Rycenga *et al.* demonstrated that polymer grafts located on certain faces of plasmonic Ag nanocubes could be selectively displaced when in contact with an elastomer stamp inked with alkanethiol molecules. When released from the stamp and allowed to assemble in aqueous solutions, the functionalized nanocubes assemble into clusters with varying dimensions, depending on how many of the nanocube sides were modified with hydrophobic ligands (Fig. 10).[46] While such approaches can generate nanoparticles that prefer to assemble in specific orientations, the utility of these techniques in the fabrication of plasmonic nanocomposites is severely limited by the ability to scale up these surface modification techniques for large nanoparticle quantities.

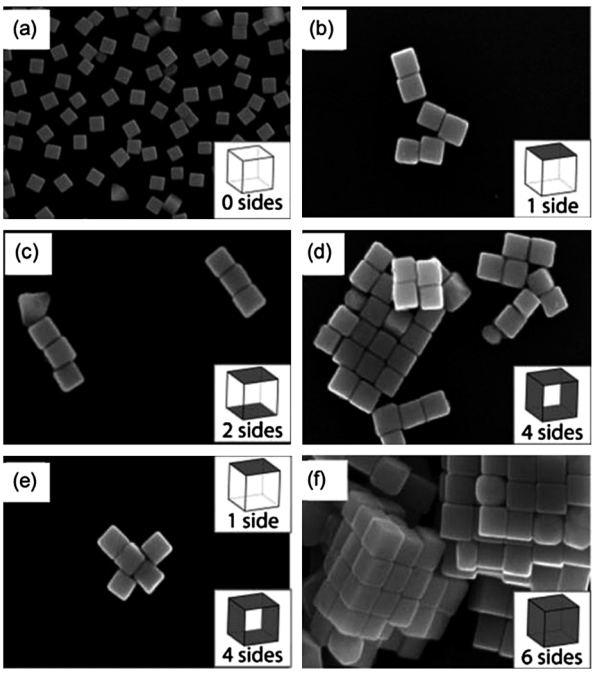

Fig. 10 SEM images of assemblies of Ag nanocubes (mean edgelength 97 ± 6 nm) in water with certain number of cube faces functionalized with hydrophobic thiolate SAMs (labeled by dark color), the remaining faces on the cube were remain hydrophilic. In (e), cubes with four hydrophobic sides were mixed with cubes that only had one hydrophobic face at a ratio of 1 : 4 and then allowed to self-assemble in water. Reproduced with permission from ref. 46.

Homogeneous surface modification

Research efforts have also demonstrated that nanoparticle assembly with controlled inter-nanoparticle orientations can be achieved by homogeneously grafting nanoparticles with polymer chains. For shaped nanoparticles, homogeneous polymer grafts can facilitate nanoparticle assembly into orientations that maximize the interaction area between neighboring nanoparticles to obtain largest attraction when the assembly is driven by depletion attraction or linkers. For example, Au nanorods coated with a homogeneous ligand shell of polymer over the entire nanorod surface is observed to form side-to-side binding conformations (where the nanorods assemble parallel to each other) that can be reinforced by molecular linkers.[47] Grzelczak and co-workers reported that this oriented nanorod clustering could also result in side-by-side nanorod orientations where the nanorods are assembled into ladder-like stacks and are slightly offset from each other. These unique structures give rise to unique "anti-bonding" surface plasmon modes in the optical absorption spectra, suggesting that these assemblies possess electromagnetic chirality.[48]

Similarly, Jones *et al.* demonstrated that shaped metal nanoparticles can be driven into oriented 3D supercrystals when homogeneously grafted with DNA strands.[49] Au nanorods, Ag triangular prisms, Ag rhombic dodecahedra, and Ag octahedral organize into face-centered cubic arrangements with inter-nanoparticle orientations that maximize hybridization interactions. While DNA strands provide strong hybridization interactions that drive assembly, this study demonstrated key design concepts that can be generalized to polymer-grafted nanoparticles that are anisotropic in shape: (i) that both nanoparticle shape and polymer grafts play synergistic roles in directing nanoparticle assembly, and (ii) that the length of the polymer graft often determines the relative importance of each parameter (shape or polymer) in directing inter-nanoparticle orientation. For DNA grafts, nanoparticles grafted with long, flexible DNA strands assemble into superstructures where inter-nanoparticle orientations are randomly generated and less influenced by nanoparticle shape.

Using linear homopolymer grafts, our research group recently demonstrated that inter-nanoparticle orientations of shaped metal plasmonic nanoparticles can be modulated by polymer graft length. Au nanorods, Ag triangular nanoprisms, and Ag nanocubes were modified by hydrophilic end-tethered polymers and embedded into a hydrophobic polymer matrix.[50] Solvent or thermal annealing of this nanocomposite drives spontaneous segregation of linear, string-like nanoparticle domains. Within these strings, inter-nanoparticle orientation is dictated by the steric interactions between polymer chains grafted on the surfaces of neighboring nanoparticles. Monte Carlo simulations predicting the free energy profile of two approaching Ag nanocubes indicate that at a critical graft chain length, polymer–polymer repulsion can be large enough to discourage close-packed nanoparticle orientations.[51] To confirm this by experiment, we modified colloidal Ag nanocubes with both ultra-long polymer grafts (~15 nm in length as determined by dynamic light scattering measurements) and

ultra-short polymer grafts (~2.0 nm in length). When grafted with long polymer chains, the nanocubes favor edge–edge (EE) orientations that alleviate the steric repulsion between adjacent, closely spaced nanocubes. In the EE configuration, nanocube assemblies produce hot spots in the interstitial junctions between nanocube edges, evidenced by broad LSPR modes in the red wavelengths and also in electrodynamic simulations (Fig. 10). When grafted with short polymer chains, the nanocubes adopt face–face (FF) orientations favored by strong van der Waals interactions. Poor electromagnetic field localization within FF assemblies results in a broadband scattering response for these nanocubes (Fig. 11).

The free energy profiles also indicate the presence of a phase transition between EE and FF configurations. We demonstrated this experimentally by thermally treating the nanoparticle–polymer composites for nanocubes grafted with various chain length polymers. As shown in Fig. 11d, nanocubes grafted with a short polymer chain switch from the edge–edge orientation (15.1 ± 1.9%) to face–face orientation (88.7 ± 1.8%). This reorientation of nanoparticles may provide a convenient strategy for designing responsive plasmonic materials where such phase transitions can be predicted by theory.

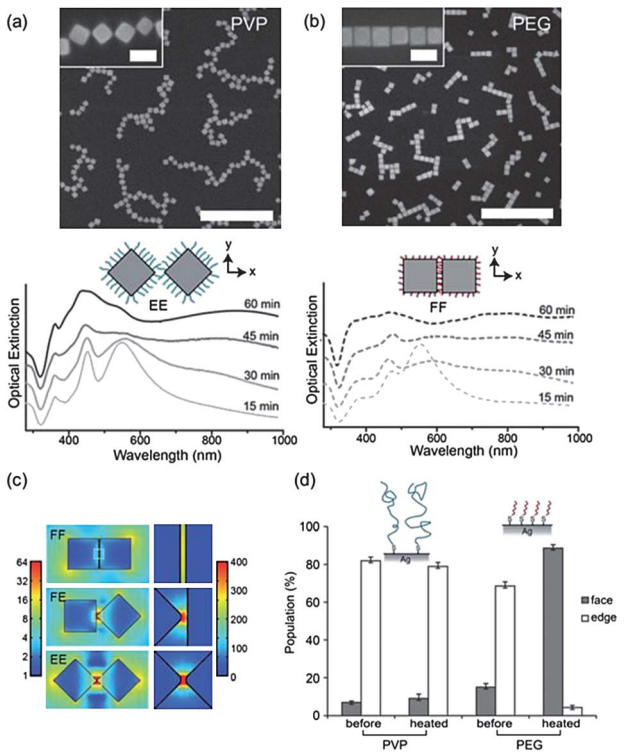

Fig. 11 SEM images and plasmonic response of oriented Ag nanocube junctions formed in PS film. (Scale bar = 1 μm, inset scale bar = 100 nm.) The extinction spectra of the nanocomposite films of Ag nanocubes modified with (a) PVP–thiol assembled in EE configuration after solvent annealing and (b) PEG–alkanethiol ligands assemble through face coordination after both solvent annealing and thermal annealing at $T > T_g$ for 4 hours. Extinction spectra were taken for samples subjected to different solvent vapor exposure times to obtain films with varying nanocube string lengths: 15 min (1 particle), 30 min (2 particles), 45 min (6 particles), and 60 min (15+ particles), showing peaks corresponding to coupled SP modes in the near-infrared. (c) Electric field strength (color) for Ag nanocubes (80 nm edgelength) with a 2 nm gap in three favored orientations: face–face (FF), face–edge (FE), and edge–edge (EE). Magnified regions of the nanojunctions (dashed box) correspond to a 20 nm × 20 nm area. The EE configuration supports the strongest field localization with a maximum field enhancement >1200E_o (incident field) at the nanocube corners. (d) The percent of edge and face coordination in nanocube assemblies before and after thermal treatment. Upon thermal annealing, PEG-grafted nanocubes rearrange from EE to the FF configuration. Reproduced with permission from ref. 51.

5 Plasmonic amphiphiles and vesicles

Hierarchical plasmonic structures can be assembled by imparting amphiphilic behavior to the surface of metal nanoparticles, where assembly is driven by the segregation of hydrophobic and hydrophilic components. Hydrophobic interactions can serve as the main driving force in the nanoparticle self-assembly process. Sánchez-Iglesias *et al.* recently developed a quantitative model that accounts for hydrophobic attractions in the solvent-induced, reversible self-assembly of PS-coated gold nanoparticles, where cluster size and interparticle spacing within the assembled 3D nanoparticle clusters are well-controlled by the addition of the amphiphilic polymer PS-*b*-PAA.[52] In these cases, electromagnetic coupling between nanoparticles is facilitated by the assembly of micelle- and vesicle-like structures. For example, Au nanorods can be selectively grafted with hydrophobic PS chains at the nanorod tips to generate an amphiphilic nanorod–polymer structure analogous to an A–B–A triblock copolymer.[42] However, site-selectivity is not a requirement; amphiphilic nanoparticles and nanorods can also be generated by randomly co-grafting both hydrophobic and hydrophilic polymer brushes onto the metal nanoparticle surface. For example, spherical Au nanoparticles grafted with both polyethylene glycol (PEG) and poly(methyl methacrylate) (PMMA) chains are capable of assembling into vesicles that possess hollow cavities around 200 nm in diameter enclosed by a thin membrane of close-packed nanoparticles.[53] Plasmonic coupling between the nanoparticles comprising the vesicle membrane undergo a red-shift of $\Delta\lambda = 30$ nm relative to the LSPR wavelength of the unassembled colloidal dispersion. Introducing a percentage of charged monomers into the PMMA graft can generate a pH-responsive vesicle, where the Au nanoparticles can be assembled with smaller gap sizes or completely disassembled into individual nanoparticles (Fig. 12a and b). Careful tuning of solvent conditions and nanoparticle size can also yield nanoparticle dimers instead of fully assembled vesicles, which give rise to two LSPRs that correlate to polarizations perpendicular and parallel to the dimer axis (Fig. 12c).[54] The same plasmonic building blocks can be assembled over large-scales into 2D membranes at oil–water interfaces, where the collective plasmonic properties of the assembly can be tailored by changing solvent conditions (Fig. 12d).[55]

Amphiphilicity can also be programmed into the nanoparticle surface by grafting block co-polymer tethers that can offer increased control over the architectural complexity of nanoparticle assemblies. Spherical Au nanoparticles grafted with amphiphilic BCPs of poly(2-(2-methoxyethoxy)ethyl methacrylate)-*block*-PS or poly(ethyl oxide)-*block*-PS have been demonstrated to self-assemble into tubular or vesicular structures[56] (Fig. 13a). Triggered by film rehydration (which is a technique commonly used for preparing vesicles of amphiphilic

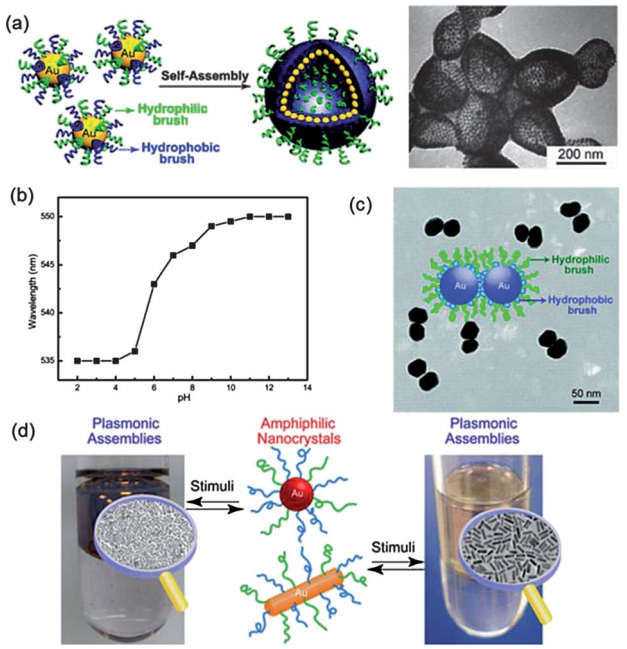

Fig. 12 (a) Schematic illustration of self-assembly of amphiphilic nanocrystals with mixed polymer brushes into vesicular structures. TEM images of the plasmonic vesicles assembled from 14 nm gold nanocrystals with mixed PEG and PMMA brushes. (b) The SP peak position of vesicles of Au@PEG/PMMAVP containing 25% 4-vinylpyridine (4VP, pK_a = 5.4) as a function of solution pH. Reproduced with permission from ref. 53. (c) TEM images and schematic illustration of the self-assembly of amphiphilic gold nanocrystals coated with PEG and PMMA mixed brushes into dimers. Reproduced with permission from ref. 54. (d) Interfacial assembly of gold nanocrystals with mixed PEG and PMMA brushes. Reproduced with permission from ref. 55.

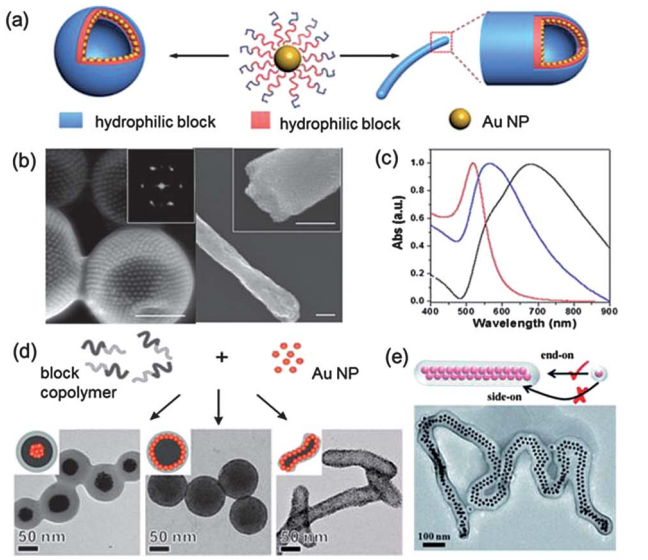

Fig. 13 (a) Schematic illustration of grafted block copolymer assisted self-assembly of amphiphilic nanocrystals into vesicles or tubules with (b) corresponding SEM images (scale bar 200 nm), respectively. Inset is the FFT pattern of SEM images of Au nanoparticle vesicles. (c) UV-vis spectra of individual Au nanoparticles (red), vesicles (blue), and tubules (black), indicating tunable plasmonic coupling of Au nanoparticle assemblies. Reproduced with permission from ref. 56. (d) Schematics illustrated assembly of PS–PAA and Au nanoparticle coated with (left) hydrophobic dodecanethiol (DT) or mixed ligands of DT and hydrophilic mercaptoundecanol (middle and right) with TEM images of the resulted composite. Reproduced with permission from ref. 59. (e) Schematics illustrating the 1D assembly of Au nanoparticle@PSPAA assisted by the sphere-to-cylinder transformation of polymer micelles with TEM images of the resulted Au nanoparticle@PSPAA double-line chains. Reproduced with permission from ref. 21a.

BCPs[57]) the grafted BCPs on the nanoparticle surface undergo conformational rearrangement to expose the hydrophilic block on the outer vesicle surface while exposing the hydrophobic blocks within the vesicle interior. Vesicle morphology and inter-nanoparticle distance within the vesicle membrane can be tuned by varying the mean length of the hydrophobic block. These plasmonic vesicles can then be loaded with payloads such as Raman reporter molecules or target biomolecules, serving as promising candidates for integrated drug delivery and SERS-active plasmonic probes.[58] Plasmonic vesicles and tubules can also be obtained by assembling BCP strands with Au nanoparticle in solution. As shown in Fig. 13d, Au nanoparticle can either segregated in the core of amphiphilic polymers micelles of PS-*b*-poly(acrylic acid) (PS-*b*-PAA) or distributed at the PS–PAA interface to reduce the interfacial energy between the two polymers, which is dictated by surface energy of the nanoparticle capping ligands.[59] Wang *et al.* reported the assembly of Au nanoparticles coated with PS-*b*-PAA chains that self-organize into extended string-of-pearl type structures that are exactly two nanoparticles wide[21a] (Fig. 13e). The observed assembly is analogous to the sphere-to-cylinder phase transition for polymer vesicles and is instigated by protonation of the PAA blocks which reduces charge repulsion between the nanoparticles. While the plasmon signatures for these long, unbranched string structures were not reported, the ability to direct the assembly of these metal nanoparticle structures with uniform widths and inter-nanoparticle spacings may be potentially useful for the bottom-up fabrication of plasmonic wires and waveguides.

6 Large-scale plasmonic nanocomposites

Recent advances in plasmonic nanoparticle–polymer composites have exploited metal nanoparticle organization within homopolymers, polymer blends, and BCP matrices. These assembly strategies have the potential to enable scalable plasmonic materials fabrication, at least in 2D. Encapsulation within a polymer matrix may also provide a convenient strategy for generating responsive plasmonic materials, since polymer thin-films tend to be mechanically flexible and can accommodate external stressors—such as thermal or solvent annealing, stretching, and swelling—that allow dynamic movement of the encapsulated nanoparticles. The same polymer matrix may also serve as a convenient dielectric medium that can be heated and cooled to freeze-capture desired nanoparticle arrangements as they evolve during the assembly process.

Miscible nanocomposites

One of the key challenges in fabricating nanocomposites with desired electromagnetic properties is controlling the spatial distribution of the nanoparticles and morphology of the assemblies in the polymer matrix. Spontaneous diffusion of

nanoparticles in blended nanocomposites is a well-studied phenomenon and can be generally understood by examining depletion–attraction forces.[60] Typically, nanoparticle dispersion within a polymer is guided by the miscibility of the two blended phases (the nanoparticle "filler" and the surrounding polymer matrix) and polymer brushes can be grafted onto the nanoparticle surface to improve their miscibility. If the brush–matrix interaction is favorable (Flory–Huggins parameter, $\chi < 0$), the free energy of mixing is reduced due to favorable contacts between the miscible grafts and matrix polymer chains and nanoparticles remain stable in their fully dispersed state.[61] Alternatively, when the brush–matrix interaction is unfavorable with $\chi > 0$, nanoparticles tend to aggregate. However, when the brush and matrix are chemically similar with $\chi = 0$, the nanoparticle dispersion depends on polymer-specific properties such as matrix chain length and surface density of the polymer grafts.[62] A "dry-brush condition" results when short polymer grafts on nanoparticle surfaces reject the relatively large matrix polymer chains; similarly, a "wet-brush" condition results when long nanoparticle grafts interdigitate with the matrix polymer.

PS-grafted spherical Au nanoparticles have been demonstrated to undergo aggregation when embedded within PS films under dry-brush conditions. Assembly results in a red-shift in the LSPR wavelength from 517 nm to 540 nm and a significantly broadened resonance compared to the LSPR for individual nanoparticles.[63] Recently, Hore *et al.* demonstrated that Au nanorods grafted with long PS chains (of length N) disperse well in a matrix of short-chain PS (of length P). Under wet-brush conditions, the films undergo little change their optical response; under dry-brush conditions at $P > 2N$, nanorods phase separate from the polymer matrix mainly through side-to-side binding motifs. This is attributed to depletion attractions (Fig. 14b and c).[64] As the matrix polymer chain length P is increased, the optical absorption peak attributed to the longitudinal LSPR mode of the nanorods is increasingly blue-shifted (Fig. 14c). This continuous shift results from increasing the number of side-by-side nanorod aggregates and enhanced electromagnetic coupling.

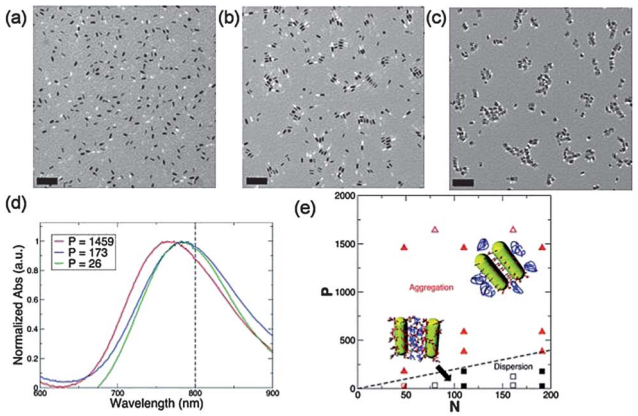

Fig. 14 Optical and dispersion characterization (TEM images) of PS grafted Au nanorods (N) in PS (P) films. (a) $N = 110$, $P = 26$; (b) $N = 110$, $P = 1459$, and (c) $N = 48$, $P = 1459$. (d) The UV-vis spectra of the composite at $N = 110$ as P increases from 26 to 1459, the dashed line is the LSPR wavelength for isolated Au nanorods in PS. (e) Dispersion map of PS grafted Au nanorods in PS films, showing how N and P determine nanorod morphology. Squares correspond to composites with isolated nanorods that are dispersed in PS, and triangles correspond to nanorods that form aggregates in PS. The morphology for the PEG grafted Au nanorod (N) in PEO(P) film is also given (open symbols). The dashed line corresponds to $P = 2N$ and represents the transition between aggregation and dispersion. Reproduced with permission from ref. 64.

Nanoparticle–polymer blend composites

A greater degree of spatial control over nanoparticle assembly can be achieved by introducing polymer-grafted nanoparticles into immiscible homopolymer blends, where the nanoparticles are enthalpically driven to the blend interface to reduce interfacial tension and stabilize microphase morphology. Much of the fundamental work on such nanocomposites has been carried out with dielectric nanoparticles. For example, Composto's group demonstrated distribution of PMMA-grafted silica nanoparticles in PMMA/poly(styrene-*ran*-acrylonitrile) (dPMMA/SAN) polymer blends after thermal annealing.[65] For increasing PMMA brush lengths, the nanoparticles first segregate to the dPMMA–SAN interface. As brush length is further increased, the nanoparticles partition between this interface and dPMMA phase before moving completely into the dPMMA phase. Russell's group demonstrated co-continuous microstructured blends of PS and poly(vinyl methyl ether) kinetically trapped by percolating networks of CdSe nanoparticles when quenched above a lower critical solution temperature.[66] Nanoparticle–polymer blends with spherical Au nanoparticles has also been demonstrated where the nanoparticles are capped with cross-linked polymer shells to accommodate thermal annealing of polytriphenylamine (PTPA) and PS blends.[67] As shown in Fig. 15a, when the nanoparticle-grafted polymer chains are neutral to both PS and PTPA phases, the nanoparticles localize at the PS–PTPA interface. While we were unable to find studies where these homopolymer blends were used to specifically align plasmonic nanostructures, this facile technique may find utility for generating large-scale optical structures in interfacial regions or boundaries.

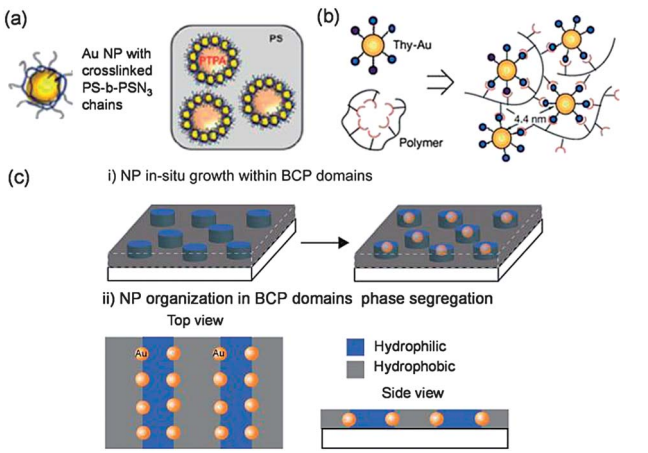

Fig. 15 Schematic illustration of film of (a) polymer blends, (b) homopolymer and (c) block copolymer guided nanoparticle assembly over large area. Reproduced with permission from ref. 67 and 69.

Nanoparticle–block copolymer composites

A more widely exploited strategy is the use of BCP templates to pattern metal nanoparticle assembly, where nanoparticles are corralled within a specific block domain or at the interface between two domains.[60,68,70] Metal nanoparticles can also be incorporated into BCPs in solution to create monolayer protected clusters that self-assemble into higher order structures.[69] Frankamp *et al.* incorporated Au nanoparticles functionalized with thymine groups into diaminotriazine-functionalized BCPs to form nanoparticle clusters that assemble due to hydrogen-bonding between the functional groups on the nanoparticle and the BCP (Fig. 15b).[69] Early work achieved periodic arrays of metal nanoparticles through *in situ* growth of the nanoparticle within a BCP film (Fig. 15c). Incorporation of metal salt into one domain of the film or within BCP micelles is typically achieved through a metal anchoring group. For example, Ag and Au metal salts can be complexed to a phosphinated polymer block and then subjected to thermal annealing to produce metal nanoclusters approximately 5.5 nm in diameter within a cylindrical polymer domain.[71] Nanoporous BCP arrays can also be generated by selective removal of one of the blocks after microphase segregation. Thayumanavan *et al.* synthesized a dithiol-linked polystyrene-*b*-poly(ethylene oxide) (PS–SS–PEO) where the removal of the cylindrical PEO revealed hollow thiol-terminated cylindrical pores. These nanopores were then decorated with Au by immersing the film in a solution of $HAuCl_4$ and carrying out chemical reduction on the surface of the pore interior.[72] Kim *et al.* used BCP thin-films to generate highly ordered planar SERS substrates by spin-casting $AgNO_3$-loaded polystyrene-*b*-poly(4-vinylpyridine) (PS-*b*-P4VP) micelles onto a support to form a hexagonally packed micellar film.[73] Reduction with $NaBH_4$ results in Ag nanoparticle clusters arranged in a hexagonal 2D array. Using PS block length to predetermine cluster spacing, they demonstrated that SERS intensity for these films increased dramatically with decreased cluster spacing.

Metal nanoparticles incorporated into BCP films can be also organized during the phase separation process as shown in Fig. 15c.[74] nanoparticle location is dictated by chemically modifying the nanoparticle surface to: (i) favor one domain by using a hydrophobic or hydrophilic ligand shell;[68b] (ii) favor the domain interface by using a mixed ligand shell;[75] or (iii) interact with an ancillary molecule that mediates the interaction between the nanoparticle and the surrounding polymer.[76] For example, Au nanoparticles grafted with end-tethered PS–thiol ligands were incorporated into a lamellar poly(styrene-*b*-2-vinylpyridine) (PS-*b*-P2VP) diblock copolymer template.[77] By decreasing the areal density of the PS grafts on the Au nanoparticle surface, a sharp transition was observed where nanoparticles migrated from the hydrophobic PS domain to the PS–P2VP interface. The effect of nanoparticle volume fraction on PS–P2VP domain morphology has been further investigated with Au–Pt core–shell nanoparticles with a cross-linked thiol-terminated poly(styrene-*b*-1,2- & 3,4-isoprene) (PS-*b*-PI-SH) graft.[78] Upon microphase separation, the Au–Pt nanoparticles are positioned at the domain interfaces within the PS-*b*-P2VP lamellar film. With an increasing volume fraction of nanoparticles, the PS-*b*-P2VP morphology transitions from lamellar sheets to a bicontinuous network during which the Au–Pt nanoparticles remain at the PS–P2VP interface. Thus, with judicious selection of the nanoparticle surface chemistry, the location of plasmonic nanoparticles within a microphase separated BCP matrix can be precisely controlled. However, one major difficulty with this strategy is that nanoparticle size is often restricted to less than the matrix polymer chain length such that the microphase separation of the BCP matrix is not disrupted.

Microphase-separated BCP film can also serve as ordered templates for patterning deposited nanoparticles.[70,79] Lee *et al.* demonstrated a thin-film of hexagonally ordered PS-*b*-P4VP as a template for citrate-stabilized Au nanoparticles (Fig. 16). These 2D hexagonal arrays were employed as SERS substrates. To increase order in the array, the pyridine groups of the P4VP domains could be cross-linked. Moreover, the SERS enhancement factor was found to change by exposing the adsorbed nanoparticle array to a metal overgrowth solution, thereby increasing nanoparticle diameter and decreasing gap distance. Choi *et al.* also utilized carbodiimide cross-linking chemistry to covalently tether Au nanoparticles to a prefabricated BCP surface.[79a] A hexagonal patterned film of PS-*b*-PMMA was used to template the deposition of Au nanoparticles capped with thioctic acid by selectively functionalizing the PMMA domains with ethylenediamine for carbodiimide linkage to the carboxyl groups on the Au nanoparticles. This nanoparticle–BCP tether provides selective immobilization of Au nanoparticles to the PMMA domains, and interparticle distance can be tuned by changing the BCP molecular weight. By selectively swelling or removing certain domains, the BCP templates have also been demonstrated as topographic templates to guide selective nanoparticle deposition into nanogrooves.[80]

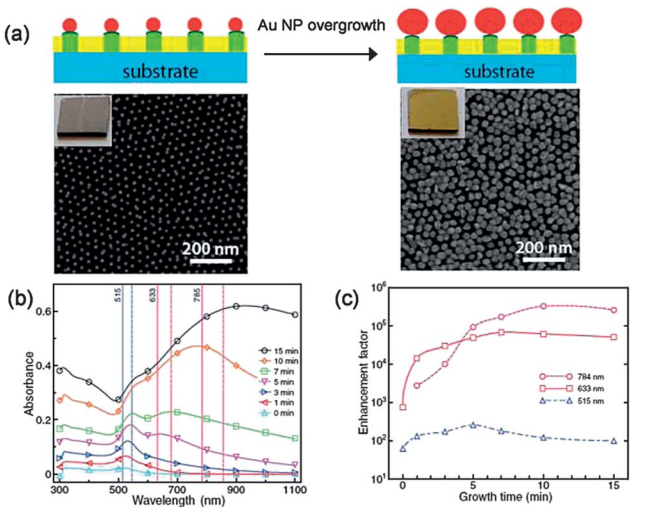

Fig. 16 (a) Schematic and SEM images of SERS substrate on silicon fabricated by Au nanoparticle deposition on quaternized PS-*b*-P4VP film template followed by nanoparticle overgrowth for 10 min, inset is the photographs of the substrate under white light illumination. (b) UV-vis attenuation spectra of SERS substrates on glass with overgrowth times ranging from 0 to 15 min. The vertical lines indicate the wavelengths of the incident (solid) and the scattered (dash) light utilized in our SERS measurements. (c) SERS substrate enhancement factors as a function of overgrowth time and probing (incident) laser wavelength. Reproduced with permission from ref. 79*b*.

7 New directions

Deformable plasmonic nanocomposites

Mechanically stretchable and flexible polymer matrices have great potential in the fabrication of responsive plasmonic nanocomposites. Older work in this area investigated colloidal nanorods and nanoparticles dispersed within PVA films, which can then be stretched or compressed to give optical absorption signatures that vary depending on the degree of plasmonic coupling within the films (Fig. 17a).[20,81] Self-actuated polymers may provide a direct route to achieving responsive plasmonic materials. Fundamental work has been carried out for plasmonic arrays fabricated by top-down methods. For example, metal nanoparticle arrays fabricated by photolithography can be deposited onto shrink-film substrates, where spacing and pitch of the nanoparticles within the array can be dilated or shrunk by either mechanical or thermal activation.[82] These macroscopic films are flexible and can accommodate curved surfaces and other arbitrary 3D geometries.[83] Bottom-up assembly of colloidal metal nanoparticles within a self-actuated composite may demonstrate large LSPR shifts and actuated polymer stretching may also serve to align or orient shaped nanoparticles within the nanocomposite.

Plasmonic fibers and textiles

Electrospinning is a highly scalable manufacturing technique that is able to produce micro- to nanoscale fibers from polymer melts and solutions. Incorporation of plasmonic nanoparticle building blocks electrospun fibers may enable unique low-dimensional nanoparticle assemblies for plasmonic fibers, with the potential for manufacturing large quantities of these materials for the fabrication of plasmonic textiles. Kim *et al.* demonstrated that Au nanoparticles could be co-spun with semicrystalline polyethylene oxide to give 1D nanoparticle arrays within polymer nanofibers[84] and Yu *et al.* showed that Ag dimers or nanoparticle aggregates could be introduced into PVA nanofibers (Fig. 17c).[85] Nanofibers that encapsulate aggregates of metal nanoparticles exhibit electromagnetic field enhancements and have been demonstrated as good SERS substrates, with enhancement factors up to 10^9.[85] More recent progress has shown that Au nanorods incorporated into polyacrylamide (PAM) fibers align uniaxially exhibit photon-to-plasmon conversion efficiencies up to 70% for waveguiding applications (Fig. 17b).[86]

Layer-by-Layer (LbL) assembly

LbL assembly is a versatile technique that can be used to incorporate plasmonic building blocks into 2D films or 3D multilayer structures. By carrying out sequential adsorption of complementary materials—in most cases, charged nanoparticles and oppositely charged polyelectrolytes—planar nanocomposites can be grown into stacked 3D materials with fine control over each successive layer. For example, negatively charged Au nanoparticles can be readily integrated within poly(styrene sulfonate) (PSS) and poly(allylamine hydrochloride) (PAH) (PAH–PSS) multilayers films by successively spin-coating the polyelectrolyte and nanoparticle layers.[87] Plasmonic coupling between different layers of Au nanoparticles (observed by measuring a redshift in the optical absorption signatures) and between nanoparticles in the same layer can be tuned by nanoparticle density and thickness of polyelectrolyte layer. In these and other studies, interlayer plasmonic coupling is effectively screened by increasing polyelectrolyte spacer layers.[88] More recently, the Norris group demonstrated that polyelectrolyte spacers between Ag nanocubes and an underlying metal film could accurately control plasmonic coupling across a

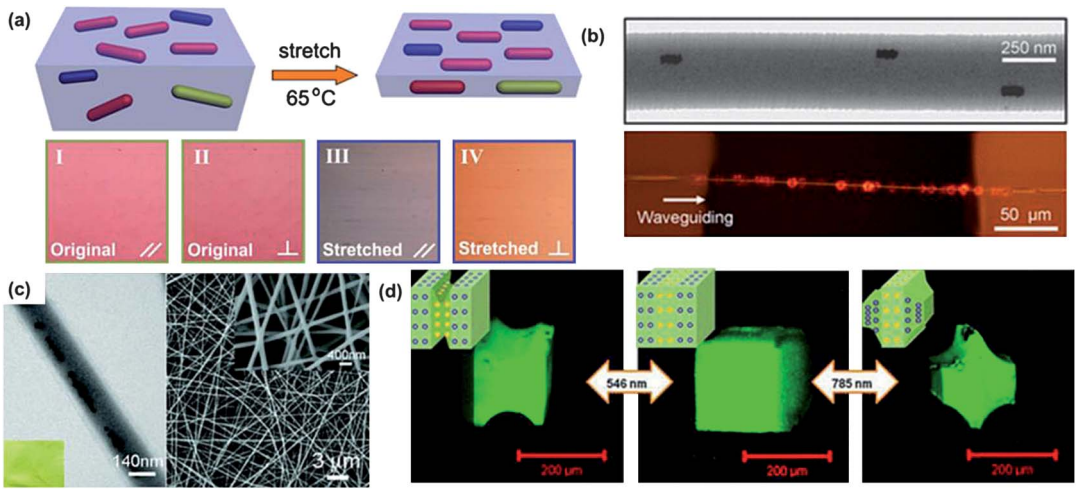

Fig. 17 (a) Schematic diagram of the stretched Au nanorod–PVA composite film process with optical microscopy images of the original and stretched film under white light illumination with polarization parallel and perpendicular to the stretch direction. Reproduced with permission from ref. 81c. (b) TEM image of Au nanorod–PVA nanofiber and its application as waveguide. Reproduced with permission from ref. 86. (c) Typical TEM and SEM image of Ag/PVA nanofibers incorporated with chain like Ag NP aggregates. Inset is the photograph of the corresponding Ag/PVA nanofiber mat. Reproduced with permission from ref. 85. (d) Confocal laser scanning microscopy images of light-controlled shape changes in 3-D NP–polymer composite, which was built by layer by layer deposition of poly(methacrylic acid) and temperature-responsive PNIPAM grafted Au nanoparticle and nanoshells. Reproduced with permission from ref. 90.

large areas, enabling the fabrication of a metasurface by simply spin-casting a dense film of nanocubes onto a polyelectrolyte-coated metal film.[89] Other interactions, such as hydrogen bonding and host–guest interactions, can be used to craft hierarchical plasmonic assemblies *via* a LbL strategy.[90] Moreover, LbL can enable the integration of multiple nanostructures within different materials strata to provide multifunctional stacked plasmonic materials (Fig. 17d).

8 Conclusions and outlook

In recent years, research directed toward the self-assembly of nanoparticle-based plasmonic materials has grown rapidly. While many of these assembly approaches are able to achieve impressive control over the formation of hierarchical nanoparticle structures and patterns, few of these approaches allow the facile integration of these nanoparticles into coatings or devices. The polymer-directed strategies discussed in this review provide a unique strategy to both control the organization of nanoparticle building blocks (by guiding interparticle separation distance, interparticle orientation, and aggregation) and to integrate the nanoparticles into functional materials using polymer fabrication techniques that take advantage of batch, low-cost processing. For applications that require large-scale material production such as metamaterial coatings and nonlinear optical films, nanocomposites will play an important if not integral role. Of particular importance is the ability to encapsulate nanoparticles into a dielectric polymer matrix to enable long-term stability of the self-assembled structures. Strategies that directly incorporate plasmonic nanoparticles into manufacturable structures – such as the plasmonic fibers discussed in the previous section – offer a practical route to achieving plasmonic textiles and scaffolds that are modular and readily configurable for applications such as optical or colorimetric sensing. Such nanoparticle–polymer composites will certainly advance the integration and utility of plasmonic nanoparticles by offering precise control over material architecture from the nano- to the macroscale.

Notes and references

1 (*a*) V. E. Ferry, L. A. Sweatlock, D. Pacifici and H. A. Atwater, *Nano Lett.*, 2008, **8**, 4391–4397; (*b*) R. A. Pala, J. White, E. Barnard, J. Liu and M. L. Brongersma, *Adv. Mater.*, 2009, **21**, 3504–3509.

2 D. R. Smith, W. J. Padilla, D. C. Vier, S. C. Nemat-Nasser and S. Schultz, *Phys. Rev. Lett.*, 2000, **84**, 4184.

3 (*a*) V. M. Shalaev, W. Cai, U. K. Chettiar, H.-K. Yuan, A. K. Sarychev, V. P. Drachev and A. V. Kildishev, *Opt. Lett.*, 2005, **30**, 3356–3358; (*b*) V. M. Shalaev, *Nat. Photonics*, 2007, **1**, 41–48.

4 S. A. Maier, P. G. Kik, H. A. Atwater, S. Meltzer, E. Harel, B. E. Koel and A. A. G. Requicha, *Nat. Mater.*, 2003, **2**, 229–232.

5 (*a*) M. I. Stockman, *Phys. Rev. Lett.*, 2004, **93**, 137404; (*b*) D. K. Gramotnev and S. I. Bozhevolnyi, *Nat. Photonics*, 2010, **4**, 83–91.

6 (*a*) L. Martin-Moreno, F. J. Garcia-Vidal, H. J. Lezec, K. M. Pellerin, T. Thio, J. B. Pendry and T. W. Ebbesen, *Phys. Rev. Lett.*, 2001, **86**, 1114; (*b*) J. Henzie, M. H. Lee and T. W. Odom, *Nat. Nanotechnol.*, 2007, **2**, 549–554.

7 (*a*) J. A. Fan, C. Wu, K. Bao, J. Bao, R. Bardhan, N. J. Halas, V. N. Manoharan, P. Nordlander, G. Shvets and F. Capasso, *Science*, 2010, **328**, 1135–1138; (*b*) N. Engheta, *Science*, 2007, **317**, 1698–1702.

8 (*a*) A. Tao, P. Sinsermsuksakul and P. Yang, *Nat. Nanotechnol.*, 2007, **2**, 435–440; (*b*) C.-F. Chen, S.-D. Tzeng, H.-Y. Chen, K.-J. Lin and S. Gwo, *J. Am. Chem. Soc.*, 2007, **130**, 824–826.

9 (*a*) A. Tao, P. Sinsermsuksakul and P. Yang, *Angew. Chem., Int. Ed.*, 2006, **45**, 4597–4601; (*b*) Y. Sun and Y. Xia, *Science*, 2002, **298**, 2176–2179.

10 X. Xia, J. Zeng, L. Oetjen, Q. Li and Y. Xia, *J. Am. Chem. Soc.*, 2012, **134**, 1793–1801.

11 A. B. R. Mayer, S. H. Hausner and J. E. Mark, *Polym. J.*, 2000, **32**, 15–22.

12 E. Katz and I. Willner, *Angew. Chem., Int. Ed.*, 2004, **43**, 6042–6108.

13 Y. Kang and T. A. Taton, *Macromolecules*, 2005, **38**, 6115–6121.

14 N. R. Jana, L. Gearheart and C. J. Murphy, *Adv. Mater.*, 2001, **13**, 1389–1393.

15 (*a*) K. Park, H. Koerner and R. A. Vaia, *Nano Lett.*, 2010, **10**, 1433–1439; (*b*) B. Nikoobakht and M. A. El-Sayed, *Chem. Mater.*, 2003, **15**, 1957–1962.

16 (*a*) P. Setua, R. Pramanik, S. Sarkar, C. Ghatak, S. K. Das and N. Sarkar, *J. Phys. Chem. B*, 2010, **114**, 7557–7564; (*b*) L. M. Bronstein, *et al.*, *Langmuir*, 2000, **16**, 3626–3632.

17 (*a*) S. Rucareanu, M. Maccarini, J. L. Shepherd and R. B. Lennox, *J. Mater. Chem.*, 2008, **18**, 5830–5834; (*b*) J. C. Love, L. A. Estroff, J. K. Kriebel, R. G. Nuzzo and G. M. Whitesides, *Chem. Rev.*, 2006, **105**, 1103–1170.

18 M. Karg, S. Jaber, T. Hellweg and P. Mulvaney, *Langmuir*, 2011, **27**, 820–827.

19 (*a*) B. P. Khanal and E. R. Zubarev, *Angew. Chem., Int. Ed.*, 2007, **46**, 2195–2198; (*b*) X. W. Zhang, L. Liu, J. Tian, J. Zhang and H. Y. Zhao, *Chem. Commun.*, 2008, 6549–6551.

20 J. Pérez-Juste, B. Rodriguez-Gonzalez, P. Mulvaney and L. M. Liz-Marzán, *Adv. Funct. Mater.*, 2005, **15**, 1065.

21 (*a*) H. Wang, L. Y. Chen, X. S. Shen, L. F. Zhu, J. T. He and H. Y. Chen, *Angew. Chem., Int. Ed.*, 2012, **51**, 8021–8025; (*b*) M. X. Yang, T. Chen, W. S. Lau, Y. Wang, Q. H. Tang, Y. H. Yang and H. Y. Chen, *Small*, 2009, **5**, 198–202.

22 D. Munoz-Rojas, J. Oro-Sole, O. Ayyad and P. Gomez-Romero, *Small*, 2008, **4**, 1301–1306.

23 S. R. Guo, J. Y. Gong, P. Jiang, M. Wu, Y. Lu and S. H. Yu, *Adv. Funct. Mater.*, 2008, **18**, 872–879.

24 (*a*) H. Duan, H. Hu, K. Kumar, Z. Shen and J. K. W. Yang, *ACS Nano*, 2011, **5**, 7593–7600; (*b*) B. Gao, K. Sarveswaran, G. Bernstein and M. Lieberman, *Langmuir*, 2009, **26**, 12680–12683.

25 H.-Y. Huang, W.-F. Chen and P.-L. Kuo, *J. Phys. Chem. B*, 2005, **109**, 24288–24294.

26 E. C. Cho, S.-W. Choi, P. H. C. Camargo and Y. Xia, *Langmuir*, 2010, **26**, 10005–10012.
27 R. Sardar and J. S. Shumaker-Parry, *Nano Lett.*, 2008, **8**, 731–736.
28 A. Lukach, K. Liu, H. Therien-Aubin and E. Kumacheva, *J. Am. Chem. Soc.*, 2012, **134**, 18853–18859.
29 X. Qian, J. Li and S. Nie, *J. Am. Chem. Soc.*, 2009, **131**, 7540–7541.
30 S. Srivastava, B. L. Frankamp and V. M. Rotello, *Chem. Mater.*, 2005, **17**, 487–490.
31 Y. Hirokawa and T. Tanaka, *J. Chem. Phys.*, 1984, **81**, 6379–6380.
32 (*a*) M. Karg, I. Pastoriza-Santos, J. Perez-Juste, T. Hellweg and L. M. Liz-Marzan, *Small*, 2007, **3**, 1222–1229; (*b*) R. Contreras-Caceres, J. Pacifico, I. Pastoriza-Santos, J. Perez-Juste, A. Fernandez-Barbero and L. M. Liz-Marzan, *Adv. Funct. Mater.*, 2009, **19**, 3070–3076.
33 M. Karg, T. Hellweg and P. Mulvaney, *Adv. Funct. Mater.*, 2011, **21**, 4668–4676.
34 J. J. Mock, M. Barbic, D. R. Smith, D. A. Schultz and S. Schultz, *J. Chem. Phys.*, 2002, **116**, 6755–6759.
35 (*a*) P. J. Schuck, D. P. Fromm, A. Sundaramurthy, G. S. Kino and W. E. Moerner, *Phys. Rev. Lett.*, 2005, **94**, 017402; (*b*) K. H. Su, Q. H. Wei, X. Zhang, J. J. Mock, D. R. Smith and S. Schultz, *Nano Lett.*, 2003, **3**, 1087–1090.
36 J. N. Israelachvili, *Intermolecular and surface forces*, Academic Press, 1992.
37 B. Nikoobakht, Z. L. Wang and M. A. El-Sayed, *J. Phys. Chem. B*, 2000, **104**, 8635–8640.
38 (*a*) M. Chen, J. Kim, J. P. Liu, H. Fan and S. Sun, *J. Am. Chem. Soc.*, 2006, **128**, 7132–7133; (*b*) J. Ren and R. D. Tilley, *J. Am. Chem. Soc.*, 2007, **129**, 3287–3291.
39 (*a*) T. K. Sau and A. L. Rogach, *Adv. Mater.*, 2010, **22**, 1781–1804; (*b*) J. Zeng, J. Tao, D. Su, Y. Zhu, D. Qin and Y. Xia, *Nano Lett.*, 2011, **11**, 3010–3015.
40 H. Kim, R. P. Carney, J. Reguera, Q. K. Ong, X. Liu and F. Stellacci, *Adv. Mater.*, 2012, **24**, 3857–3863.
41 J. He, M. T. Perez, P. Zhang, Y. J. Liu, T. Babu, J. L. Gong and Z. H. Nie, *J. Am. Chem. Soc.*, 2012, **134**, 3639–3642.
42 Z. Nie, D. Fava, E. Kumacheva, S. Zou, G. C. Walker and M. Rubinstein, *Nat. Mater.*, 2007, **6**, 609–614.
43 A. Lee, G. F. S. Andrade, A. Ahmed, M. L. Souza, N. Coombs, E. Tumarkin, K. Liu, R. Gordon, A. G. Brolo and E. Kumacheva, *J. Am. Chem. Soc.*, 2011, **133**, 7563–7570.
44 T. Chen, H. Wang, G. Chen, Y. Wang, Y. Feng, W. S. Teo, T. Wu and H. Chen, *ACS Nano*, 2010, **4**, 3087–3094.
45 (*a*) B. B. Wang, B. Li, B. Zhao and C. Y. Li, *J. Am. Chem. Soc.*, 2008, **130**, 11594–11595; (*b*) J. H. Yoon, J. Lim and S. Yoon, *ACS Nano*, 2012, **6**, 7199–7208.
46 M. Rycenga, J. M. McLellan and Y. Xia, *Adv. Mater.*, 2008, **20**, 2416–2420.
47 (*a*) A. McLintock, N. Hunt and A. W. Wark, *Chem. Commun.*, 2011, **47**, 3757–3759; (*b*) T. S. Sreeprasad, A. K. Samal and T. Pradeep, *Langmuir*, 2008, **24**, 4589–4599.
48 M. Grzelczak, S. A. Mezzasalma, W. H. Ni, Y. Herasimenka, L. Feruglio, T. Montini, J. Perez-Juste, P. Fornasiero, M. Prato and L. M. Liz-Marzan, *Langmuir*, 2012, **28**, 8826–8833.
49 M. R. Jones, R. J. Macfarlane, B. Lee, J. A. Zhang, K. L. Young, A. J. Senesi and C. A. Mirkin, *Nat. Mater.*, 2010, **9**, 913–917.
50 B. Gao, Y. Alvi, D. Rosen, M. Lav and A. R. Tao, *Chem. Commun.*, 2013, **49**, 4382–4384.
51 B. Gao, G. Arya and A. R. Tao, *Nat. Nanotechnol.*, 2012, **7**, 433–437.
52 A. Sánchez-Iglesias, M. Grzelczak, T. Altantzis, B. Goris, J. Pérez-Juste, S. Bals, G. V. Tendeloo, S. H. Donaldson Jr, B. F. Chmelka, J. N. Israelachvili and L. M. Liz-Marzán, *ACS Nano*, 2012, **6**, 11059–11065.
53 J. Song, L. Cheng, A. Liu, J. Yin, M. Kuang and H. Duan, *J. Am. Chem. Soc.*, 2011, **133**, 10760–10763.
54 L. Cheng, J. Song, J. Yin and H. Duan, *J. Phys. Chem. Lett.*, 2011, **2**, 2258–2262.
55 L. Cheng, A. Liu, S. Peng and H. Duan, *ACS Nano*, 2010, **4**, 6098–6104.
56 J. He, Y. Liu, T. Babu, Z. Wei and Z. Nie, *J. Am. Chem. Soc.*, 2012, **134**, 11342–11345.
57 B. M. Discher, Y.-Y. Won, D. S. Ege, J. C.-M. Lee, F. S. Bates, D. E. Discher and D. A. Hammer, *Science*, 1999, **284**, 1143–1146.
58 J. Song, J. Zhou and H. Duan, *J. Am. Chem. Soc.*, 2012, **134**, 13458–13469.
59 Q. Luo, R. J. Hickey and S.-J. Park, *ACS Macro Lett.*, 2013, **2**, 107–111.
60 A. C. Balazs, T. Emrick and T. P. Russell, *Science*, 2006, **314**, 1107–1110.
61 M. J. A. Hore and R. J. Composto, *ACS Nano*, 2010, **4**, 6941–6949.
62 (*a*) J. Kim and P. F. Green, *Macromolecules*, 2010, **43**, 1524–1529; (*b*) P. Akcora, H. Liu, S. K. Kumar, J. Moll, Y. Li, B. C. Benicewicz, L. S. Schadler, D. Acehan, A. Z. Panagiotopoulos, V. Pryamitsyn, V. Ganesan, J. Ilavsky, P. Thiyagarajan, R. H. Colby and J. F. Douglas, *Nat. Mater.*, 2009, **8**, 354–359.
63 M. K. Corbierre, N. S. Cameron, M. Sutton, K. Laaziri and R. B. Lennox, *Langmuir*, 2005, **21**, 6063–6072.
64 M. J. A. Hore, A. L. Frischknecht and R. J. Composto, *ACS Macro Lett.*, 2012, **1**, 115–121.
65 H. Chung, K. Ohno, T. Fukuda and R. J. Composto, *Nano Lett.*, 2005, **5**, 1878–1882.
66 L. Li, C. Miesch, P. K. Sudeep, A. C. Balazs, T. Emrick, T. P. Russell and R. C. Hayward, *Nano Lett.*, 2011, **11**, 1997–2003.
67 T. Kwon, T. Kim, F. B. Ali, D. J. Kang, M. Yoo, J. Bang, W. Lee and B. J. Kim, *Macromolecules*, 2011, **44**, 9852–9862.
68 (*a*) M. R. Bockstaller, R. A. Mickiewicz and E. L. Thomas, *Adv. Mater.*, 2005, **17**, 1331–1349; (*b*) J. J. Chiu, B. J. Kim, E. J. Kramer and D. J. Pine, *J. Am. Chem. Soc.*, 2005, **127**, 5036–5037; (*c*) S. Gupta, Q. Zhang, T. Emrick and T. P. Russell, *Nano Lett.*, 2006, **6**, 2066–2069; (*d*) Y. Lin, A. Boker, J. He, K. Sill, H. Xiang, C. Abetz, X. Li, J. Wang, T. Emrick, S. Long, Q. Wang, A. Balazs and T. P. Russell, *Nature*, 2005, **434**, 55–59.
69 B. L. Frankamp, O. Uzun, F. Ilhan, A. K. Boal and V. M. Rotello, *J. Am. Chem. Soc.*, 2002, **124**, 892–893.
70 R. W. Zehner, W. A. Lopes, T. L. Morkved, H. Jaeger and L. R. Sita, *Langmuir*, 1998, **14**, 241–244.

71 Y. N. C. Chan, R. R. Schrock and R. E. Cohen, *J. Am. Chem. Soc.*, 1992, **114**, 7295–7296.
72 J.-H. Ryu, S. Park, B. Kim, A. Klaikherd, T. P. Russell and S. Thayumanavan, *J. Am. Chem. Soc.*, 2009, **131**, 9870–9871.
73 W. J. Cho, Y. Kim and J. K. Kim, *ACS Nano*, 2012, **6**, 249–255.
74 Y. Lin, V. K. Daga, E. R. Anderson, S. P. Gido and J. J. Watkins, *J. Am. Chem. Soc.*, 2011, **133**, 6513–6516.
75 Q. Li, J. He, E. Glogowski, X. Li, J. Wang, T. Emrick and T. P. Russell, *Adv. Mater.*, 2008, **20**, 1462–1466.
76 Y. Zhao, K. Thorkelsson, A. J. Mastroianni, T. Schilling, J. M. Luther, B. J. Rancatore, K. Matsunaga, H. Jinnai, Y. Wu, D. Poulsen, J. M. J. Frechet, A. Paul Alivisatos and T. Xu, *Nat. Mater.*, 2009, **8**, 979–985.
77 B. J. Kim, J. Bang, C. J. Hawker and E. J. Kramer, *Macromolecules*, 2006, **39**, 4108–4114.
78 S. G. Jang, B. J. Kim, C. J. Hawker and E. J. Kramer, *Macromolecules*, 2011, **44**, 9366–9373.
79 (*a*) J. H. Choi, S. M. Adams and R. Ragan, *Nanotechnology*, 2009, **20**, 065301–065306; (*b*) W. Lee, S. Y. Lee, R. M. Briber and O. Rabin, *Adv. Funct. Mater.*, 2011, **21**, 3424–3429.
80 J. G. Son, W. K. Bae, H. Kang, P. F. Nealey and K. Char, *ACS Nano*, 2009, **3**, 3927–3934.
81 (*a*) C. J. Murphy and C. J. Orendorff, *Adv. Mater.*, 2005, **17**, 2173–2177; (*b*) B. M. I. van der Zande, L. Pages, R. A. M. Hikmet and A. v. Blaaderen, *J. Phys. Chem. B*, 1999, **103**, 5761–5767; (*c*) J. Li, S. Liu, Y. Liu, F. Zhou and Z.-Y. Li, *Appl. Phys. Lett.*, 2010, **96**, 263103.
82 M. H. Lee, M. D. Huntington, W. Zhou, J.-C. Yang and T. W. Odom, *Nano Lett.*, 2011, **11**, 311–315.
83 B. M. Ross, L. Y. Wu and L. P. Lee, *Nano Lett.*, 2011, **11**, 2590–2595.
84 G. M. Kim, A. Wutzler, H. J. Radusch, G. H. Michler, P. Simon, R. A. Sperling and W. Parak, *Chem. Mater.*, 2005, **17**, 4949–4957.
85 D. He, B. Hu, Q.-F. Yao, K. Wang and S.-H. Yu, *ACS Nano*, 2009, **3**, 3993–4002.
86 P. Wang, L. Zhang, Y. Xia, L. Tong, X. Xu and Y. Ying, *Nano Lett.*, 2012, **12**, 3145–3150.
87 C. Jiang, S. Markutsya and V. V. Tsukruk, *Langmuir*, 2004, **20**, 882–890.
88 (*a*) N. Malikova, I. Pastoriza-Santos, M. Schierhorn, N. A. Kotov and L. M. Liz-Marzán, *Langmuir*, 2002, **18**, 3694–3697; (*b*) S. Vial, I. Pastoriza-Santos, J. Pérez-Juste and L. M. Liz-Marzán, *Langmuir*, 2007, **23**, 4606–4611.
89 A. Moreau, C. Ciracì, J. J. Mock, R. T. Hill, Q. Wang, B. J. Wiley, A. Chilkoti and D. R. Smith, *Nature*, 2012, **492**, 86–89.
90 Z. C. Zhu, E. Senses, P. Akcora and S. A. Sukhishvili, *ACS Nano*, 2012, **6**, 3152–3162.